



LAWRENCE  
LIVERMORE  
NATIONAL  
LABORATORY

# Neodymium Fluorescence Quenching by Hydroxyl Groups in Phosphate Laser Glasses

*P. R. Ehrmann, K. Carlson, J. H. Campbell, C.  
A. Click, R. K. Brown*

**September 2, 2003**

University Conference on Glass Science  
Troy, New York, August 13-15, 2003

This document was prepared as an account of work sponsored by an agency of the United States Government. Neither the United States Government nor the University of California nor any of their employees, makes any warranty, express or implied, or assumes any legal liability or responsibility for the accuracy, completeness, or usefulness of any information, apparatus, product, or process disclosed, or represents that its use would not infringe privately owned rights. Reference herein to any specific commercial product, process, or service by trade name, trademark, manufacturer, or otherwise, does not necessarily constitute or imply its endorsement, recommendation, or favoring by the United States Government or the University of California. The views and opinions of authors expressed herein do not necessarily state or reflect those of the United States Government or the University of California, and shall not be used for advertising or product endorsement purposes.

## Neodymium fluorescence quenching by hydroxyl groups in phosphate laser glasses

P. R. Ehrmann, K. Carlson\* and J. H. Campbell†  
University of California, Lawrence Livermore National Laboratory  
7000 East Avenue, L-491, Livermore, California 94550  
(925) 422-6497, (925) 423-0792 (fax), campbell12@llnl.gov

C. A. Click\*\* and R. K. Brow  
University of Missouri at Rolla  
222 McNutt Hall  
Rolla, Missouri 65409

### Abstract

Non-radiative losses due to OH fluorescence quenching of the Nd<sup>3+</sup> <sup>4</sup>F<sub>3/2</sub> state are quantified over a range of OH concentrations from  $4 \times 10^{18}/\text{cm}^3$  to  $4 \times 10^{20}/\text{cm}^3$  and Nd doping levels from 0.4 to  $9 \times 10^{20}/\text{cm}^3$  in two K<sub>2</sub>O-MgO-Al<sub>2</sub>O<sub>3</sub>-P<sub>2</sub>O<sub>5</sub> metaphosphate glasses having different K/Mg ratios (~1/1 and 2/1). The quenching rate is found to vary linearly with the Nd and OH concentrations as predicted by Forster-Dexter theory. However, in contrast to theory the OH quenching rate extrapolates to a non-zero value at low Nd<sup>3+</sup> doping levels. It is proposed that at low Nd<sup>3+</sup> concentrations the OH is correlated with Nd sites in the glass. The quenching strength of OH on a per ion basis is found to be weak compared to other common transition metal impurities (e.g. Fe<sup>2+</sup>, Co<sup>2+</sup>, Ni<sup>2+</sup>, Cu<sup>2+</sup>). Nevertheless, OH dominates the Nd quenching in phosphate glass because under most processing conditions OH is present at concentrations  $10^2$  to  $10^3$  greater than transition metal ion impurities. A correlation of the quenching strength of OH and common metal impurity ions with the degree of spectral overlap of the impurity absorption bands and the four <sup>4</sup>F<sub>3/2</sub> to <sup>4</sup>I<sub>j</sub> transitions shows good agreement.

**PACS codes: 42.70-a**

**Key words: Laser glass, neodymium, fluorescence, phosphate glass, hydroxyl in glass**

### 1. Introduction

Currently, all major high-energy ( $\geq 1$  kJ) solid-state laser systems in the US, Europe and Asia use Nd-phosphate glasses as the gain medium [1]. In some cases the quantity of glass

†To whom all correspondence should be addressed: campbell12@llnl.gov

\*Current address: Alfred University, Alfred, NY

\*\*Current address: Schott Glass Technologies, Duryea, PA

installed in the laser is very large. For example, the 1.8 MJ, 500 TW solid-state laser currently under construction at Lawrence Livermore National Laboratory (LLNL) requires nearly  $1.3 \times 10^5$  kg of finished Nd-phosphate glass in the form of 3072 thick plates ( $80 \times 45 \times 4$  cm<sup>3</sup>) [2,3]. The reason Nd-doped phosphate glasses are widely used is because they have excellent energy storage and extraction characteristics [1,4-7] and can be made in large sizes, with high optical quality and free of damage causing inclusions [3,8-9].

One factor that degrades the performance of Nd-doped laser glasses is the presence of OH impurities [1,10-12]. The upper laser level for Nd<sup>3+</sup> is the metastable  $^4F_{3/2}$  state and the rate of energy transfer from this state is given by the inverse of the fluorescence lifetime ( $\tau_f^{-1}$ )[10,13-15]. Hydroxyl groups reduce the lifetime (increase the decay rate) [1,10,12,15] and thereby reduce the stored energy in the  $^4F_{3/2}$  state resulting in a corresponding degradation in the laser output energy. Phosphate glass hosts are particularly vulnerable to OH contamination because they tend to readily absorb water during melting [3,16]. Consequently, sophisticated processing methods are used to dehydroxylate both the glass melt and the glass raw materials [16]. Despite these efforts, some residual hydroxyl groups remain in the glass typically at concentrations greater than 100ppm.

Results from a number of Nd-OH quenching studies on a wide range of different phosphate glass compositions with different Nd concentrations have recently been compiled [1,10]. Although the OH quenching rate shows the theoretically expected linear dependence with Nd concentration at high doping levels, upon extrapolation to low Nd concentrations the quenching rate exhibits unexpected behavior in that the rate appears to plateau, becoming independent of the Nd concentration (see Fig. 9 in ref. 1). Unfortunately the data upon which this observation is based is from a wide range of different glass compositions reported by different investigators. Thus the question remains as to whether a single glass composition would exhibit this same behavior; to our knowledge there has not been a systematic study of fluorescence quenching over a wide range of both OH and Nd concentrations for a given base glass composition. In this paper

we report the results of such a study on two K<sub>2</sub>O-MgO-Al<sub>2</sub>O<sub>3</sub>-P<sub>2</sub>O<sub>5</sub> metaphosphate glasses (Table 1). One glass is compositionally similar to a readily available commercial laser glass and the second has a different modifier mix-ratio and variable rare earth content. The purpose of using these two glasses is to examine whether a change in the base glass composition affects the OH quenching behavior.

The quenching data reported here are given in terms of a useful correlation that can be directly input to laser amplifier design codes and used to reliably predict the effect of quenching over a wide range of Nd doping levels and residual OH concentrations. The quenching strength by OH is also compared with that of other common impurities in laser glass and it is shown that the quenching strength correlates with the degree of spectral overlap between the energy donor (Nd<sup>3+</sup>) and acceptor (impurity) as predicted by Förster-Dexter theory[13,17-18]. In addition, we offer an explanation for the unusual behavior of the Nd<sup>3+</sup> quenching rate by OH at low Nd concentrations.

## 2. Nd-fluorescence quenching: governing equations

The rate of energy transfer ( $k$ ) from the Nd<sup>3+</sup> <sup>4</sup>F<sub>3/2</sub> state can be written as [10]

$$k = k_{\text{rad}}(1-f_{\text{trap}}) + k_{\text{nonrad}} \quad (1)$$

where  $k_{\text{rad}}$  and  $k_{\text{nonrad}}$  are the radiative and non-radiative decay rates (Hz), respectively and  $f_{\text{trap}}$  is the fraction of emitted radiation that is “trapped” within the sample. Radiation trapping simply refers to the re-absorption and re-emission of the laser ion fluorescence due to the finite sample size and doping density. The fraction of trapped radiation,  $f_{\text{trap}}$ , can be calculated for Nd-doped phosphate glasses using the expression [10,19]

$$f_{\text{trap}} = \beta_{880}\Omega_{880}[1 - \exp(-\alpha\ell_{\text{eff}})] \quad (2)$$

where  $\beta_{880}$  is the fluorescence branching ratio for the <sup>4</sup>F<sub>3/2</sub>-to-<sup>4</sup>I<sub>9/2</sub> transition at 880 nm and  $\Omega_{880}$  is the fractional spectral overlap of the 880 nm absorption and emission bands. The term in square brackets accounts for the probability of photon re-absorption in the finite-sized sample where  $\alpha$  is the absorption coefficient at 880 nm and  $\ell_{\text{eff}}$  the effective optical pathlength [19]. The 880 nm

absorption coefficient is calculated from the product of the Nd-doping level [Nd] (ions/cm<sup>3</sup>) and the absorption cross-section ( $\sigma$ ) at 880 nm (cm<sup>2</sup>). Recent work has shown that  $\ell_{\text{eff}}$  can be accurately estimated for a wide range of sample geometries by  $V^{1/3}$  where V is the sample volume (cm<sup>3</sup>) [10].

The radiative decay rate,  $k_{\text{rad}}$ , is a fundamental property of the material and is the sum of the individual radiative decay rates from <sup>4</sup>F<sub>3/2</sub> state to the manifold of <sup>4</sup>I<sub>j</sub> states. Typically  $k_{\text{rad}}$  is determined using the Judd-Ofelt (J-O) treatment [20] of spectral intensities however errors that enter into this analysis can lead to uncertainties of  $\geq 15\%$  in the predicted values. The radiative decay rate can also be independently determined from the measured fluorescence decay using Eq. (1) provided all non-radiative quenching and radiation trapping effects can be quantified. In this study we use this latter approach.

The non-radiative decay rate ( $k_{\text{nonrad}}$  in Eq. (1)) is a sum of contributions from all non-radiative processes [1,10]

$$k_{\text{nonrad}} = k_{\text{mp}} + k_{\text{Nd}} + k_{\text{OH}} + \sum_{i=1}^n k_{\text{TMi}} + \sum_{j=1}^m k_{\text{REj}}. \quad (3)$$

The first term in Eq.3 refers to multi-phonon relaxation ( $k_{\text{mp}}$ ) and is an intrinsic loss that depends on the highest phonon energy of the glass matrix [13,21]. The contribution due to multi-phonon decay can be computed from the expression

$$k_{\text{mp}} = A \exp(-\alpha_{\text{mp}} \Delta E) \quad (4)$$

where  $\Delta E$  is the energy difference between the Nd<sup>3+</sup> <sup>4</sup>F<sub>3/2</sub> and <sup>4</sup>I<sub>15/2</sub> states (5500 cm<sup>-1</sup>) and A and  $\alpha_{\text{mp}}$  are empirically derived constants for a particular glass matrix, in this case phosphate [21]. Values for A and  $\alpha_{\text{mp}}$  have been reported to be  $2.4 \times 10^{12}$  Hz and  $4.35 \times 10^{-3}$  cm, respectively based on fitting Eq. 4 to measured values of the Nd<sup>3+</sup> multiphonon decay rates in phosphate glasses published by various sources [1].

The second term in Eq. 3 is the contribution due to Nd self-quenching and refers to the energy exchange between Nd ions [10,13,22]. This is a well-studied area with numerous reports

of compositional effects on Nd self-quenching in a wide variety of glasses (see for example [1] and references cited therein).

The last three terms represent non-radiative losses due to impurities that enter during glass processing, particularly hydroxyl groups ( $k_{OH}$ ), transition metals ( $k_{TM}$ ) and rare earths ( $k_{RE}$ ). Since there can be several transition-metal or rare-earth impurities in a given glass, then the losses are expressed in Eq. 3 as a sum of the individual impurity ion contributions [10].

The rate of energy transfer between  $Nd^{3+}$  and an impurity ion, or between two  $Nd^{3+}$  ions, is described by a resonant dipole-dipole interaction using the model originally formulated by Förster [17] and later extended by Dexter [18]. In the Förster-Dexter model,  $Nd^{3+}$  is the “donor” (D) and the impurity ion is the “acceptor” (A); the energy transfer rate is given as [13,23]

$$k_{DA} = \eta R_{DA}^{-6} \int \frac{G_D(\nu) K_A(\nu) d\nu}{\nu^4} \quad (5)$$

where  $\eta$  is a constant for a given base glass composition and  $R_{DA}$  is the inter-nuclear distance between donor and acceptor. The integral describes the spectral overlap between the donor emission,  $G_D(\nu)$ , and acceptor absorption,  $K_A(\nu)$ , where  $\nu$  is in wave numbers. The spectral overlap term is constant for a given donor-acceptor pair, allowing one to rewrite Eq. (5) as [13]

$$k_{DA} = CR_{DA}^{-6} \quad (6)$$

where C is a constant.

If the donor and acceptor ions are homogeneously distributed through the glass then the  $R_{DA}^{-6}$  dependence in Eq. 6 can be expressed in terms of the ion concentrations in the experimentally more useful form:

$$k_{DA} = C'[D][A] \quad (7)$$

where C' is an empirically derived constant and [D] and [A] are the donor and acceptor ion concentrations, respectively. Thus, the Förster-Dexter theory offers a straightforward method for correlating impurity-quenching measurements with the impurity (acceptor) and lasant ion (donor)

concentrations. Note also that the Förster-Dexter theory (Eq. 7) predicts zero impurity quenching rates upon extrapolation to zero donor or acceptor concentration.

### 3. Experimental procedure

#### 3.1 Glass preparation and analysis

Two sets of glass samples were prepared for this study (Table 1). One set (KMAP (2:1)) was formulated with a composition similar to that reported for the commercially available laser glass, LG-770 [24]. The  $K_2O/MgO$  ratio for this suite of glasses is 2.3-to-1 (+/- 0.3). The Nd concentration was varied while holding the total rare earth content constant by using a mixture of  $La_2O_3$  and  $Nd_2O_3$  (Table 1). The second set of glass samples (the KMAP (1:1) series) was purposely formulated to have a different composition while maintaining the same cation mix. Specifically the  $K_2O/MgO$  ratio was held near unity (1-to-1, +/- 0.04) and the  $Nd_2O_3$  content was varied without compensating with  $La_2O_3$ . The analyzed glass compositions given in Table 1 are accurate to +/-5% of the value reported.

The KMAP (2:1) samples were prepared from a series of seven cullet glasses each containing a different Nd doping level between 0.4 to  $8.9 \times 10^{20}/cm^3$  (see Table 1). The cullet batches were melted at 1200°C in fused silica crucibles using a platinum stirrer to achieve compositional homogeneity. The original cullet melts were dehydroxylated by bubbling dry  $O_2$  through the melt as well as by flowing it across the melt surface. This achieved OH contents based on measured absorption at  $3000\text{ cm}^{-1}$  of  $\lesssim 1.5\text{ cm}^{-1}$  ( $\lesssim 140\text{ ppm}$ ).

These cullet glasses were then re-melted under various water vapor pressures to achieve the desired range in OH content. Specifically, about 100g of cullet was melted in a covered Pt crucible and a quartz tube was used to bubble oxygen through the melt at a flow rate of 1L/minute after it had passed through a temperature-controlled water bath held at a constant temperature between 10°C to 50°C. The oxygen was saturated with water vapor at a pressure determined by the water bath temperature. By bubbling this saturated  $O_2$  through the melt for 15 minutes, the final OH content (i.e. absorption at  $3000\text{ cm}^{-1}$ ) could be varied from about 1.5 to  $30\text{ cm}^{-1}$ .

For the KMAP (1:1) series, a single rare-earth-free cullet glass with an approximate molar composition of  $60\text{P}_2\text{O}_5-10\text{Al}_2\text{O}_3-15\text{K}_2\text{O}-15\text{MgO}$  was melted at  $1300^\circ\text{C}$ , refined at  $1350^\circ\text{C}$ , and poured at  $1100^\circ\text{C}$ . Neodymium phosphate was subsequently added to this cullet at five different  $\text{Nd}^{3+}$  doping levels between  $0.4$  to  $7.7 \times 10^{20}/\text{cm}^3$  (see Table 1).

The Nd-containing cullets were re-melted at  $1100^\circ\text{C}$  using 50-gram melts in a 100 ml silica crucible covered with a silica lid. The hydroxyl content was varied by bubbling dry oxygen gas through a distilled water bath at temperatures  $0$ ,  $25$ ,  $50$  and  $75^\circ\text{C}$  and then through the melt for 1 hour at the rate of  $0.1\text{L}/\text{minute}$ . The lowest hydroxyl levels were obtained by bubbling the melt with dry oxygen gas; a dry argon cover gas was also flowed over the melt. The final OH content, as measured by the absorption at  $3000 \text{ cm}^{-1}$ , ranged from about  $2$  to  $40 \text{ cm}^{-1}$ .

The Nd concentration in the glasses was determined using a lithium metaborate fusion procedure followed by analysis of the fusion product with inductively coupled plasma mass spectroscopy (ICP-MS; Hewlett-Packard Model 4500). The procedure involved first acid cleaning the samples followed by hand grinding to a fine particle size using a boron carbide mortar and pestle. About 50 mg of the prepared sample and 300 mg lithium metaborate were mixed in a platinum crucible and heated for 30 min. at  $1050^\circ\text{C}$ . The fused product was dissolved in dilute nitric acid and then analyzed by ICP-MS with Pr as an internal standard. The measured Nd ion concentrations in the glasses fell within 15% of the as-batched compositions.

The transition metal and rare earth ion impurity concentrations were measured using either ICP emission spectroscopy (Thermo Iris Model 6943) or ICP-MS on a glass sample fully dissolved in a perchloric acid solution. Be, and/or Pr were used as internal standards depending on the analyte.

### ***3.2 Infrared spectroscopic measurements***

Optical transmission measurements were carried out using a Fourier transform infrared spectrometer (Perkin Elmer Spectrum 2000). Polished samples with thicknesses varying from about  $0.25 \text{ mm}$  to  $5 \text{ mm}$  were used to capture the spectrum from  $370$  to  $7800 \text{ cm}^{-1}$ .

The hydroxyl concentrations were determined from the absorption coefficient measured at 3000 cm<sup>-1</sup> relative to the background absorption at 5000 cm<sup>-1</sup> and computed using the exponential form of Beer's law:

$$\alpha_{3000\text{cm}^{-1}} = -\ell n\left(T_{3000\text{cm}^{-1}} / T_{5000\text{cm}^{-1}}\right) / \ell \quad (8)$$

where T is transmission (%),  $\ell$  is the sample thickness (cm) and  $\alpha_{3000\text{cm}^{-1}}$  is the absorption coefficient at 3000 cm<sup>-1</sup>.

### 3.3 *Nd<sup>3+</sup> Fluorescence decay measurements*

Polished glass cubes (nominally 0.5 to 2.0 cm<sup>3</sup>) were fabricated from each of the melted glasses for fluorescent lifetime measurement. The sample under test was held in an anodized mount and illuminated with the broadband spectral output (~300 to 1100 nm) from a flashlamp (EG&G LS1130-4) having a 2.2  $\mu$ s pulse width. Two optical filters (Melles Griot KG-3 and BG-18) effectively blocked all but the visible pump wavelengths (340-620 nm). A photomultiplier tube (Hamamatsu R5108) mounted perpendicular to the flashlamp monitored the fluorescence signal. An optical filter on the photomultiplier (Melles Griot RG-850) blocked the pump light and allowed transmission of the fluorescence signal. The temporal decay of the signal was recorded on an oscilloscope (Tektronix TDS 380); a signal generator (Tucker Electronics, TFG 8140) was used to trigger the flashlamp and oscilloscope. The measured decay signal was fit to a single exponential function to determine the characteristic Nd<sup>3+</sup> fluorescence decay time. We also determined the decay time based on the integrated signal and found that this compared well with the exponential fit ( $\pm 5\%$ ); this provided a verification of assumed exponential behavior of the fluorescence decay. The measured data are reported here as decay rates which are the inverse of the decay times.

## 4. Results

### 4.1 *Infrared Absorption*

Fig. 1 shows a typical infrared absorption spectrum for one of the glasses used in this study; the data span the spectral range from 2400 to 6400 cm<sup>-1</sup> (4167 to 1562 nm). The spectrum in Fig.

1 is fit with four gaussian bands representing the OH transitions listed in Table 1; the results of the spectral band fit are discussed further in Section 5.

The infrared data have also been used to calculate the OH concentration in the glass samples using a conversion factor of 92 ppm per  $\text{cm}^{-1}$  absorption at  $3000 \text{ cm}^{-1}$ . This conversion has an estimated uncertainty of  $\pm 20\%$  and is based on results reported by Ehrmann and Campbell [10] for a commercial potassium magnesium aluminophosphate glass (LG-770). This factor agrees well with the value of  $100 \text{ ppm/cm}^{-1}$  at  $2900 \text{ cm}^{-1}$  reported by Houde-Walter et al. [25] for a sodium aluminophosphate glass. The conversion constant, in combination with the sample densities (Table 1), can also be used to compute the hydroxyl concentration as OH groups per  $\text{cm}^3$  and from this the absorption cross-sections given in Fig. 1. For example, for a glass density of  $2.6 \text{ g/cm}^3$  the OH concentration corresponding to  $1 \text{ cm}^{-1}$  absorption at  $3000 \text{ cm}^{-1}$  is 92 ppm or  $8.5 \times 10^{18} \text{ OH/cm}^3$ . Thus the glass shown in Fig.1 has an absorption coefficient of  $20.9 \text{ cm}^{-1}$  at  $3000 \text{ cm}^{-1}$ , corresponding to an OH concentration of about 1920 ppm or  $1.8 \times 10^{20} \text{ OH/cm}^3$ .

#### **4.2 Measured $\text{Nd}^{3+} \ ^4\text{F}_{3/2}$ decay rates and contributions from various non-radiative sources**

Fig 2. shows examples of the raw Nd fluorescence decay rate data plotted vs. OH concentration for each of the two base glass compositions used in this study (KMAP (2:1) and (1:1)). Each data point represents the measured fluorescence decay rate ( $\tau^{-1}$ ) for one of the product glasses having a given OH and Nd doping concentration. A total of twelve different Nd-doping levels were prepared for the two glasses (see Table 1). For each of the Nd-doping levels, between six to twelve different OH concentrations were prepared and the fluorescence decay rate was measured for each. The entire sample set consists of 87 different glass melts.

The OH quenching rate,  $k_{\text{OH}}$ , at a given Nd concentration was determined from the measured decay rate after removing the contributions due to radiation trapping and the non-radiative effects as given in Eqs. 1-3; specifically this includes the Nd-self quenching and multi-phonon decay. The non-radiative decay contributions due to transition metal and rare earth impurities (see Eq. 3) are negligible for the glasses prepared in this study because of the purity of

the glass melts. The analyzed impurity levels were less than 2 ppm for the strongest fluorescence quenching elements (Cu, Fe, V, Co, Ni). Based on published quenching rates for these impurities [10], the maximum possible contribution to the decay rate is less than 5 Hz for all metal ion impurities combined.

The Nd self-quenching rate was determined from a set of melts having a variable Nd concentration but a fixed sample volume and a constant as well as low OH content. The fixed sample volume assures that the radiation trapping is essentially constant for all the samples and easily accounted for [10]. Similarly, the small contribution due to OH quenching can also be easily corrected for [1,10]. The Nd self-quenching rates in the KMAP (2:1) and (1:1) glasses are shown in Fig. 3. The rate varies linearly with the square of the Nd concentration as predicted by theory (Eq. 7) where the donor and acceptor ions are both Nd.

The Nd self-quenching rate is often characterized in terms of a critical concentration,  $C_{Nd}$  that simply represents the Nd concentration at which the decay rate is twice the intrinsic radiative decay. In general, the higher the  $C_{Nd}$  value the less sensitive the glass is to concentration quenching. The measured  $C_{Nd}$ -values for the KMAP (2:1) and (1:1) glasses are  $10.3 \pm 0.3$  and  $8.5 \pm 0.3 \times 10^{20}$  ions/cm<sup>3</sup>, respectively. These values compare well with values reported for commercial laser glasses having similar compositions [1, 10]. Extrapolation of the quenching data in Fig. 3 to zero Nd gives the radiative decay rate for the glass. The radiative decay rates,  $k_{rad}$  (and radiative lifetimes,  $\tau_{rad}$ ) for the KMAP (2:1) and (1:1) glasses are 3085 Hz (324 $\mu$ s) and 2581 Hz (387  $\mu$ s), respectively.

The contribution due to radiation trapping was determined via Eq. 2 using the measured absorption coefficient at 880 nm ( $\alpha$ ) and the effective path length ( $\ell_{eff}$ ) determined from the sample volume. We use previously reported values of the branching ratio,  $\beta_{880}$ , and fractional spectral overlap,  $\Omega_{880}$ [10]. We have found that among the suites of meta-phosphate laser glasses having K, Mg, or K, Ba modifiers these values are nearly constant[1,10].

After accounting for the contributions due to radiation trapping, Nd-self-quenching and multiphonon decay, the remaining non-radiative decay is due to OH in the glass. Typical data are shown in Fig. 4 for the KMAP (2:1) and (1:1) glasses at two different Nd-doping levels. The slopes of the lines fit to the data give the quenching rate in units of Hz per  $\text{cm}^{-1}$  absorption by OH at  $3000 \text{ cm}^{-1}$ . Figure 5 summarizes the measured OH quenching rate as a function of the Nd-doping density for both glasses. Each data point represents a quenching rate determined from the slope of plots such as those in Fig. 4. To within experimental error, the data in Fig. 5 for the two glasses can be fit with the single expression

$$Q_{\text{OH}} (\text{Hz}/\text{cm}^{-1}) = a + b [\text{Nd}] \quad (9)$$

where  $Q_{\text{OH}}$  is the fluorescence quenching rate by OH in units of Hz per  $\text{cm}^{-1}$  absorption at  $3000 \text{ cm}^{-1}$  and  $[\text{Nd}]$  is the doping level in units of  $10^{20} \text{ ions}/\text{cm}^3$ . The constants  $a$  and  $b$  were determined from a linear least-squares fit to the data in Fig. 5 and have values of  $23 (+/- 2) \text{ Hz}/\text{cm}^{-1}$  and  $24 (+/- 1) \text{ Hz}/\text{cm}^{-1}$  per  $10^{20} \text{ ions}/\text{cm}^3$  of Nd-doping, respectively.

## 5. Discussion

### 5.1 OH infrared absorption spectra

The infrared absorption by OH in various glass types has been a subject of interest for many years and, in fact, the mode assignment for specific absorption bands continues to be debated [26]. In this section we simply report the observed infrared absorption bands for the glasses in this study. Of particular interest to the work here is the magnitude of the absorption at the Nd emission band near  $1800 \text{ nm}$  ( $\sim 5560 \text{ cm}^{-1}$ ) since it is the primary pathway for non-radiative loss.

Figure 1 shows the results of fitting four gaussian bands to the measured infrared absorption spectrum. The four bands were chosen based on spectral features that are OH concentration dependent and are observed in the absorption spectrum as indicated by the arrows in the figure. Table 2 summarizes the key characteristics of these four bands. The broad distribution of OH band intensities is attributed to variations in hydrogen-bonding with bridging

and non-bridging oxygens and the weak bands above about 4000cm<sup>-1</sup> are usually assigned to either combination and/or overtone vibrations [see for example ref 26 and references cited therein]. We assume the weak band near 4810 cm<sup>-1</sup> is a combination band although the accuracy of this assignment does not impact the results of this study.

The most important aspect of the infrared data for the work reported here is the measurement of the absorption cross-section at the Nd<sup>3+</sup> <sup>4</sup>F<sub>3/2</sub> to <sup>4</sup>I<sub>15/2</sub> transition at 5560 cm<sup>-1</sup> (1800nm). This is because the absorption cross-section at this wavelength governs the strength of the resonant interaction with the excited Nd<sup>3+</sup> and therefore the rate of Nd<sup>3+</sup> non-radiative energy transfer to OH vibrational modes. The absorption cross-section at 5560 cm<sup>-1</sup> is 0.15 × 10<sup>-20</sup> cm<sup>2</sup>/OH; note also that relative to this, the OH absorption intensity is negligible at the other three Nd<sup>3+</sup> <sup>4</sup>F<sub>3/2</sub> to <sup>4</sup>I<sub>J</sub> transitions near 7700, 9520 and 11,360 cm<sup>-1</sup>. Consequently, the quenching by OH is dominated by the resonant overlap at 5560 cm<sup>-1</sup>. This is discussed further in section 5.3 where the quenching strength of OH is compared with that due to common transition metal impurities.

## 5.2 Nd<sup>3+</sup> <sup>4</sup>F<sub>3/2</sub> fluorescence quenching by OH

Figure 6 compares the measured OH quenching rate from this study with data compiled by Campbell and Suratwala [1] from other literature sources; this compilation is based on data for eighteen glasses comprised of eight different near-meta-phosphate glass compositions with various Nd doping levels. The agreement between the data sets is very good and equation 9 (solid line in Fig. 6) provides an accurate representation of all the data.

It is also clear from the data in Fig. 6 that the glass modifier composition has little effect on the Nd<sup>3+</sup> quenching rate by OH. Using Förster-Dexter theory (Eq. 5) as a basis for the quenching description one can draw several conclusions regarding this insensitivity to glass composition. First, the degree of spectral overlap between the Nd emission bands and OH absorption at 1800nm must remain about the same within this group of phosphate glasses. This is reasonable because it is well known that the modifier composition has little impact on the Nd emission

wavelength within a given network former [1,27]. The insensitivity of the Nd<sup>3+</sup> emission energies/intensities to the modifier composition is because the Nd 4f orbitals are well shielded by the overlying 6s<sup>2</sup> and 5p<sup>6</sup> shells; therefore the states arising from the 4f configurations are only mildly affected by the surroundings [13,28].

In regard to the OH absorption bands, the network former, rather than the modifier, has the greater impact on the band intensity and transition energy. This is because the OH bands are influenced by hydrogen bonding to the bridging and non-bridging oxygens of the network [27]. Thus the insensitivity of the spectral overlap to the modifier mix in the phosphate glasses is not unexpected. In addition, the OH quenching is driven mainly by the spectral overlap with the Nd <sup>4</sup>F<sub>3/2</sub> to <sup>4</sup>I<sub>15/2</sub> transition at 1800nm. The OH only affects this one Nd<sup>3+</sup> transition because the OH band intensity at the other three <sup>4</sup>F<sub>3/2</sub> to <sup>4</sup>I<sub>J</sub> transitions (at 880, 1053 and 1300nm) is negligible and therefore the overlap is insignificant.

The distribution of OH within the glass matrix is generally believed to be random, however the finite quenching rate observed upon extrapolation to “zero” Nd concentration (Fig. 7) suggests that some of the OH may be correlated with Nd sites. This is illustrated by re-writing Eq. 9 for the OH quenching rate, Q<sub>OH</sub>, in terms of the OH-induced non-radiative decay rate, k<sub>OH</sub>

$$k_{OH} = \alpha_{OH} Q_{OH} \quad (10a)$$

$$= a \alpha_{OH} + b [Nd] \alpha_{OH} \quad (b)$$

$$= a' [OH] + b' [Nd][OH] \quad (c)$$

where  $\alpha_{OH}$  is the absorption coefficient at 3000 cm<sup>-1</sup> and [Nd] and [OH] are the Nd and OH concentrations in the glass (cm<sup>-3</sup>). The constants a' and b' are the a and b values given by Eq. 9 but expressed directly in units of OH concentration, that is: 27 Hz/(10<sup>19</sup> OH/cm<sup>3</sup>) and 28Hz/(10<sup>19</sup> OH/cm<sup>3</sup>) per 10<sup>20</sup> Nd/cm<sup>3</sup>, respectively. Note that the second term of Eq. 10c is equivalent to the expression given by F-D theory (i.e. Eq. 7). However the first term predicts a non-zero quenching rate upon extrapolation to “zero” Nd concentration. Within the framework of F-D theory this would imply that at low Nd concentrations there is a correlation between the Nd<sup>3+</sup>

with OH sites in the glass. In other words, the data suggests that it may be energetically favorable for the OH to coordinate with the Nd sites, particularly at low Nd-doping concentrations.

### 5.3 *OH quenching strength vs. other impurities*

Recently it has been shown that the Nd fluorescence quenching strength of various transition metal and rare-earth impurity ions in phosphate glasses correlates with the degree of spectral overlap of the  ${}^4F_{3/2}$ -to- ${}^4I_J$  emission bands with the impurity absorption in accordance with Förster-Dexter theory (Eq. 5) [10]. The data for several of the more common transition metal impurities are presented in Fig. 7 and compared to the quenching strength of OH reported here. The quenching strength is given in units of Hz per  $10^{20}$  impurity ions/cm<sup>3</sup>. The spectral overlap represents the sum of the overlap of the impurity absorption bands with the four Nd<sup>3+</sup>  ${}^4F_{3/2}$ -to- ${}^4I_J$  transitions, and is reported as the overlap normalized to that for the strongest quencher, Cu<sup>2+</sup>.

It is interesting to note that on a per ion basis the quenching rate by OH is the lowest of the impurities shown. This is counter to the common belief that OH is a strong Nd fluorescence quencher. The reason for the misconception is that the concentration of OH in the glass is generally much greater than the other impurities. Thus the quenching contribution from OH generally exceeds that of all other impurities combined. For example, a “dry” laser glass typically has an absorption at 3000 cm<sup>-1</sup> of 1-2 cm<sup>-1</sup> which is equivalent to  $\sim 10^{19}$  OH/cm<sup>3</sup>. In contrast, the concentrations of transition metal impurities in most commercial Nd-doped phosphate glasses are generally less than  $10^{16}$ - $10^{17}$  ions/cm<sup>3</sup> [3]. Thus it is clear that the quenching contribution due to OH can be attributed to its high relative concentration and not the inherent quenching strength.

The reason for low quenching strength by OH compared to the other impurities is two-fold. First the OH absorption weakly overlaps primarily the 1800 nm  ${}^4F_{3/2}$  to  ${}^4I_{15/2}$  band whereas most of the other ions have significant absorption over two or more bands (see Fig. 8 in ref. 10). In addition, the strength of the OH absorption cross-section at 1800 nm is only  $\sim 10^{-21}$  cm<sup>2</sup> because it

is a weak overtone or combination band. In contrast the cross-sections of the transition metals typical are of order  $10^{-20}$  to  $10^{-19}$  cm<sup>2</sup>/ion.

## 6.0 Conclusions

The rate of Nd<sup>3+</sup> fluorescence quenching by OH varies linearly with Nd concentration in agreement with the Förster-Dexter theory. However, in contrast to theory, at low Nd concentrations the quenching does not tend toward zero but rather attains a finite value. This suggests a possible correlation of OH with Nd<sup>3+</sup> sites implying such structural arrangements may be energetically more favored.

Comparison of quenching measurements reported here with measurements reported for other phosphate glass compositions made over much smaller Nd-doping ranges show good agreement. This leads to the general conclusion that the OH quenching rate is largely insensitive to glass composition for glasses having near-metaphosphate compositions (O/P $\approx$ 3). Therefore the quenching relationship reported here should be broadly applicable to this class of important laser glasses, particularly the most widely used commercial phosphate laser glasses (e.g. LHG-8, LG-770, LG-750).

There is the longstanding misconception that OH is a strong fluorescence quencher. Data presented here show in fact that the quenching by OH on a per-ion basis is about 10 $\times$  smaller than that for several common transition metal impurities (e.g. Cu, Fe, Ni, Co). This misconception arises because OH impurities occur at much higher concentrations compared to other impurities in phosphate glasses. For example, even the “driest” laser glasses typically have OH concentrations near 100 ppm ( $\sim 10^{19}$ /cm<sup>3</sup>). In contrast, transition metal impurities can generally be controlled to a level of a few parts-per-million with the use of high purity raw materials and reasonable care to exclude impurities during melting. Therefore the effect of the very high OH concentration off-sets its relatively weak per-ion quenching strength leading to the overall dominant quenching character of hydroxyl groups in Nd phosphate glasses.

## Acknowledgements

The authors gratefully acknowledge J. Hayden and N. Wyckoff at Schott Glass for preparation of the cullet glasses used in this study. The assistance of R. Steele and F. Zaka with certain aspects of the experiments and the useful discussions with T. Suratwala are also appreciated. This work was performed by the auspices of the U.S. Department of Energy by the University of California, Lawrence Livermore National Laboratory under Contract No. W-7405-Eng-48.

## References

- [1] J. H. Campbell and T. I. Suratwala, "Nd-doped Phosphate Glasses for High-Energy/High-Peak-Power Lasers", *J. Non-Cryst. Solids*, 263&264 (2000) 318.
- [2] E. Moses, J. Campbell, S. Stolz and C. Wuest, "The National Ignition Facility: The World's Largest optics and Laser System", *SPIE vol. 5001* (2003) p.1
- [3] J. Campbell, T. Suratwala, C. Thorsness, J. Hayden, A. Thorne, A. Marker, K. Takeuchi, M. Smolley, and G. Ficini-Dorn, "Continuous Melting of Nd-doped Phosphate Laser Glasses", *J. Non-Cryst. Solids*, 263&264 (2000) 342.
- [4] W. Koechner, *Solid-State Laser Engineering*, 4th Ed., Springer, New York (1996).
- [5] J. L. Emmett, W. F. Krupke, and J. B. Trenholme, "The Future Development of High-Power Solid State Laser Systems", Lawrence Livermore National Laboratory Report UCRL-53344, 1982.
- [6] J. T. Hunt and D. R. Speck, "Present and Future Performance of the Nova Laser System", *Opt. Eng.* 28 (1989) 461.
- [7] B. M. VanWanterghem, J. R. Murray, J. H. Campbell, D. R. Speck, C. E. Barker, I. C. Smith, D. F. Browning, and W. C. Behrendt, "Performance of a Prototype, Large-aperture Multipass Nd-Glass Laser for Inertial Confinement Fusion", *Appl. Opt.* 36 (1997) 4932.
- [8] J. H. Campbell, E. P. Wallerstein, J. S. Hayden, D. L. Sapak, D. E. Warrington, and A. J. Marker, "Effects of Melting Conditions on Platinum-Inclusion Content in Phosphate Laser Glasses", *Glastech. Ber. Glass Sci. Technol.* 68 (1995) 11.
- [9] J. H. Campbell, E. P. Wallerstein, H. Toratani, H. E. Meissner, S. Nakajima, and T. S. Izumitani, "Effects of Process Gas Environment on Platinum-Inclusion Density and Dissolution Rate in Phosphate Laser Glasses", *Glastech. Ber. Glass Sci. Technol.* 28 (1995) 59.
- [10] P. R. Ehrmann and J. H. Campbell, "Non-radiative losses and radiation trapping in Nd-doped phosphate laser glasses", *J. Am. Ceram. Soc.* 85 (2002) 1061.
- [11] H. Toratani, PhD thesis, Kyoto University, Kyoto, Japan, 1989.
- [12] H. Ebendorff-Heidepreim, W. Seeber, and D. Ehrt, "Spectroscopic Properties of Nd<sup>3+</sup> ions in Phosphate Glasses," *J. Non-Cryst. Solids*, 183 (1995) 191.
- [13] R. C. Powell, *Physics of Solid-State Laser Materials*, Springer-Verlag, New York, 1998.
- [14] Y. Jiang, S. Jiang, and Y. Jiang, "Spectral Properties of Nd<sup>3+</sup> in Aluminophosphate Glasses", *J. Non-Cryst. Solids* 112 (1989) 286.
- [15] C. Jiang, W. Gao, D. Zhuo, J. Zhang, "Effect of OH group on laser performance and physical properties of phosphate laser glass", *J. Chin. Ceram. Soc.*, 26 (1998) 97.
- [16] C. B. Thorsness, T. I. Suratwala, R. A. Steele, J. H. Campbell, J. S. Hayden, S. A. Pucilowski, and K. Suzuki, "Dehydroxylation of Phosphate Laser Glass", *SPIE vol 4102* (2000) 175.

- [17] T. Förster, "Energy Transfer and Fluorescence Between Molecules", *Ann. Phys.* 2 (1948) 56.
- [18] D. L. Dexter, "A Theory of Sensitized Luminescence in Solids", *J. Chem. Phys.* 21(1953) 836.
- [19] C. D. Marshall, S. A. Payne, L. K. Smith, H. T. Powell, W. F. Krupke, and B. H. T. Chai, "1.047- $\mu\text{m}$  Yb:Sr<sub>5</sub>(PO<sub>4</sub>)<sub>3</sub>F Energy Storage Optical Amplifier", *IEEE J. Selected Topics in Quantum Electron.* 1 (1995) 67.
- [20] W. Krupke, *IEEE J. Quantum Electron.* QE-10 (1974) 450.
- [21] C. B. Layne, W. H. Lowdermilk, and M. J. Weber, "Multiphonon Relaxation of Rare-Earth Ions in Oxide Glasses", *Phys. Rev. B.* 16 (1977) 110.
- [22] J. Caird, A. Ramponi, and P. Staver, "Quantum Efficiency and Excited-State Relaxation Dynamics in Neodymium-doped Phosphate Laser Glasses", *J. Opt. Soc. Am. B* 8 (1991) 1391.
- [23] H. Toratani, H. E. Meissner, T. Izumitani, S. E. Stokowski, "Phosphate Laser Glass of Absorption Loss of  $10^{-4}\text{cm}^{-1}$ ", *J. Non-Cryst. Solids* 95-96 (1987) 701.
- [24] Laser Glass Product Catalog, Schott Glass Technologies, Duryea PA, 1999, p.1
- [25] S. N. Houde-Walter, P. M. Peters, J. F. Stebbins and Q. Zeng, "Hydroxyl-contents and hydroxyl-related concentration quenching in erbium-doped aluminophosphate, aluminosilicate, and fluorosilicate glass", *J. Non-Cryst. Solids* 286 (2001) 118.
- [26] D. P. Zarubin, "Infrared Spectra of Hydrogen Bonded Hydroxyl Groups in Silicate Glasses. A Re-interpretation", *Phys. Chem. Glasses*, 40 (1999) 184.
- [27] S.E. Stokowski, R.A. Saroyan, M.J. Weber, *Laser glass: Nd-doped glass spectroscopic and physical properties*, Lawrence Livermore National Laboratory Report M-095, Rev. 2, vols 1&2, 1981.
- [28] S. Hufner, *Optical Spectra of Transparent Rare Earth Compounds*, Academic Press, New York, 1978.

**Table 1. Compositions (as analyzed) and densities for the two suites of Nd-doped K<sub>2</sub>O-MgO-Al<sub>2</sub>O<sub>3</sub>-P<sub>2</sub>O<sub>5</sub> (KMAP) glasses used in this study.**

melt designation	Composition (mol%) +/- 5%						Nd <sup>3+</sup> Doping (+/- 5%) (x10 <sup>20</sup> ions/cm <sup>3</sup> )	density (g/cm <sup>3</sup> )	O/P ratio
	K <sub>2</sub> O	MgO	Al <sub>2</sub> O <sub>3</sub>	P <sub>2</sub> O <sub>5</sub>	Nd <sub>2</sub> O <sub>3</sub>	La <sub>2</sub> O <sub>3</sub>			
<b>I. KMAP (2:1)</b>									
1	19.0	8.7	7.3	61.3	0.2	3.5	0.43	2.68	3.00
2	18.7	9.0	7.2	61.5	0.4	3.3	0.86	2.68	2.99
3	18.9	8.3	7.2	62.5	0.7	2.9	1.7	2.68	2.98
4	18.3	9.3	7.4	61.5	1.5	2.1	3.6	2.69	2.98
5	18.5	7.3	7.7	62.7	2.3	1.5	5.4	2.69	2.98
6	17.9	7.5	7.8	62.9	3.1	0.7	7.2	2.70	2.98
7	19.4	7.5	7.2	62.2	3.7	0.0	8.9	2.69	2.98
<b>II. KMAP (1:1)</b>									
1	14.6	14.8	9.6	60.8	0.2	0.0	0.43	2.56	2.98
2	14.6	14.8	9.5	60.8	0.3	0.0	0.90	2.56	3.00
3	14.6	14.8	9.7	60.4	0.6	0.0	1.5	2.57	3.00
4	14.1	14.6	9.2	60.7	1.4	0.0	3.6	2.61	3.01
5	13.3	13.9	8.7	61.0	3.0	0.0	7.7	2.70	3.01

**Table 2. Observed OH infrared band energies and absorption strengths.**

<b>energy*</b> <b>(cm<sup>-1</sup>)</b>	<b>Wavelength*</b> <b>(nm)</b>	<b>absorption</b> <b>cross-section*</b> <b>(x10<sup>-19</sup> cm<sup>2</sup>/OH)</b>	<b>bandwidth</b> <b>FWHM (cm<sup>-1</sup>)</b>	<b>integrated</b> <b>absorption</b> <b>(normalized)</b>
2800	3570	15.0	920	1.000
3450	2900	0.70	1010	0.053
4200	2380	0.30	645	0.011
4810	2080	0.30	1200	0.020

\* at peak intensity

## Figure Captions

Figure 1. Typical infrared spectrum of a phosphate glass used in this study showing the absorption coefficient (and cross-section) vs. energy (and wavelength) from (a) 2400 to 4400  $\text{cm}^{-1}$  and (b) from 3200 to 6400  $\text{cm}^{-1}$ ; note the 10X magnified vertical scale for the data in (b). The cross-section values are based on the OH concentration and only apply to the OH absorption. The dotted lines represent the four gaussian bands fit to the data and the dashed line is the sum of four band intensities illustrating the quality of the fit.

Figure 2. Typical raw data showing the measured Nd  ${}^4\text{F}_{3/2}$  fluorescence decay rate vs. OH concentration for KMAP (a) (1:1) and (b) (2:1) glasses; the Nd doping levels are given in the figure. The non-radiative decay contributions due to Nd self-quenching and multiphonon relaxation have not been removed from these measurements. The lines represent linear least squares fits to the data; the measurement error is within the size of the symbols except where otherwise shown.

Figure 3. Measured non-radiative decay rate due to Nd self-quenching in KMAP (a) (2:1) and (b) (1:1) glasses. The lines are linear least-squares fits to the data; the measurement error is within the size of the symbols except where otherwise shown.

Figure 4. Non-radiative decay rate due Nd fluorescence quenching by OH in KMAP (a) (2:1) and (b) (1:1) glasses at two different Nd doping levels. The lines represent linear least squares fits to the data and the slopes are the fluorescence quenching rates ( $Q_{\text{OH}}$ ) per OH impurity concentration given as  $\text{Hz}/\text{cm}^{-1}$  absorption at 3000  $\text{cm}^{-1}$ .

Figure 5. Nd fluorescence quenching by OH groups,  $Q_{\text{OH}}$ , as a function of Nd-doping concentration for both the KMAP (2:1) and (1:1) glasses. The line is a least squares fit to the data and has a slope of 24

Hz/cm<sup>-1</sup> per 10<sup>20</sup> Nd ions/cm<sup>3</sup> and a non-zero intercept of 23 Hz/cm<sup>-1</sup> where cm<sup>-1</sup> is the unit of the OH absorption coefficient at 3000 cm<sup>-1</sup>.

Figure 6. Comparison of the Nd quenching rates by OH reported here with data for eighteen other near-metaphosphate glasses as compiled elsewhere [1]; the solid line is from Fig 5.

Figure 7. Strength of Nd-fluorescence quenching by OH and other common transition metal impurities in phosphate laser glass versus the spectral overlap with the <sup>4</sup>F<sub>3/2</sub> to <sup>4</sup>I<sub>J</sub> transitions (normalized to that for Cu); data for the metal ion impurities are from [10]. The units of the quenching strength are Hz per 10<sup>20</sup> impurity ions/cm<sup>3</sup> per 10<sup>20</sup> Nd ions/cm<sup>3</sup>.

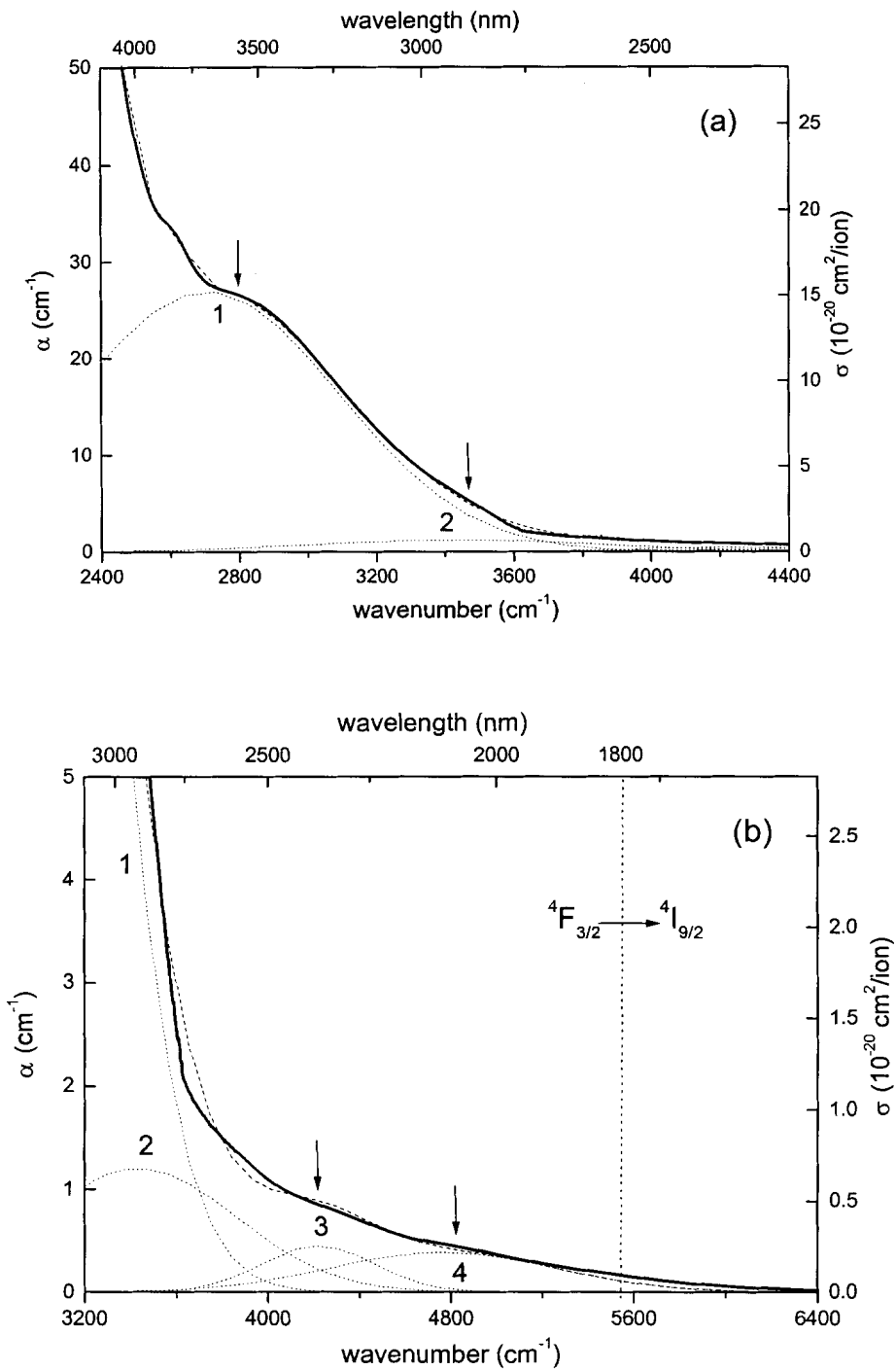


Figure 1. Typical infrared spectrum of a phosphate glass used in this study showing the absorption coefficient (and cross-section) vs. energy (and wavelength) from (a) 2400 to 4400 cm<sup>-1</sup> and (b) from 3200 to 6400 cm<sup>-1</sup>; note the 10X magnified vertical scale for the data in (b). The cross-section values are based on the OH concentration and only apply to the OH absorption. The dotted lines represent the four gaussian bands fit to the data and the dashed line is the sum of four band intensities illustrating the quality of the fit.

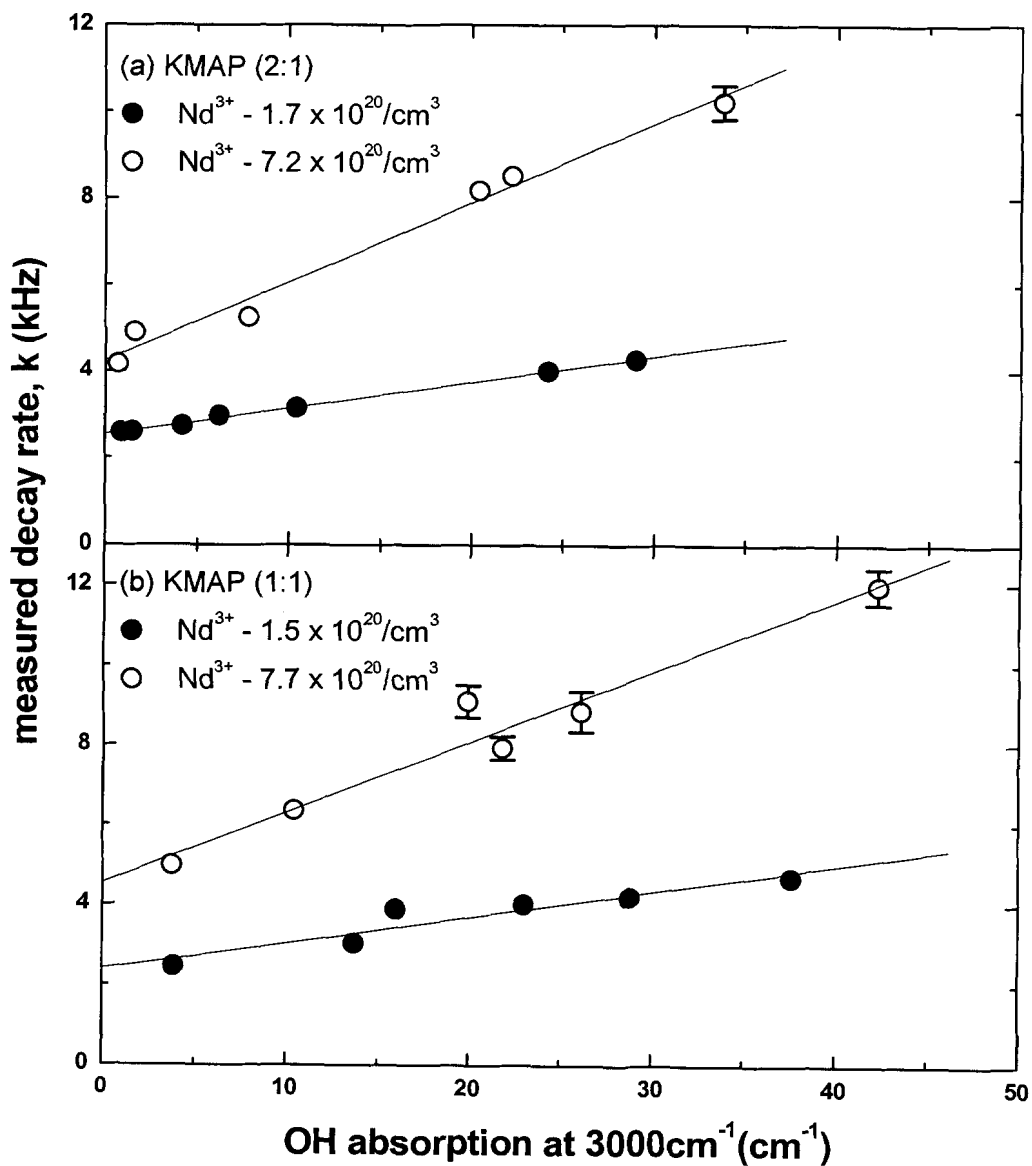


Figure 2. Typical raw data showing the measured  $\text{Nd } ^4\text{F}_{3/2}$  fluorescence decay rate vs. OH concentration for KMAP (a) (1:1) and (b) (2:1) glasses; the Nd doping levels are given in the figure. The non-radiative decay contributions due to Nd self-quenching and multiphonon relaxation have not been removed from these measurements. The lines represent linear least squares fits to the data; the measurement error is within the size of the symbols except where otherwise shown.

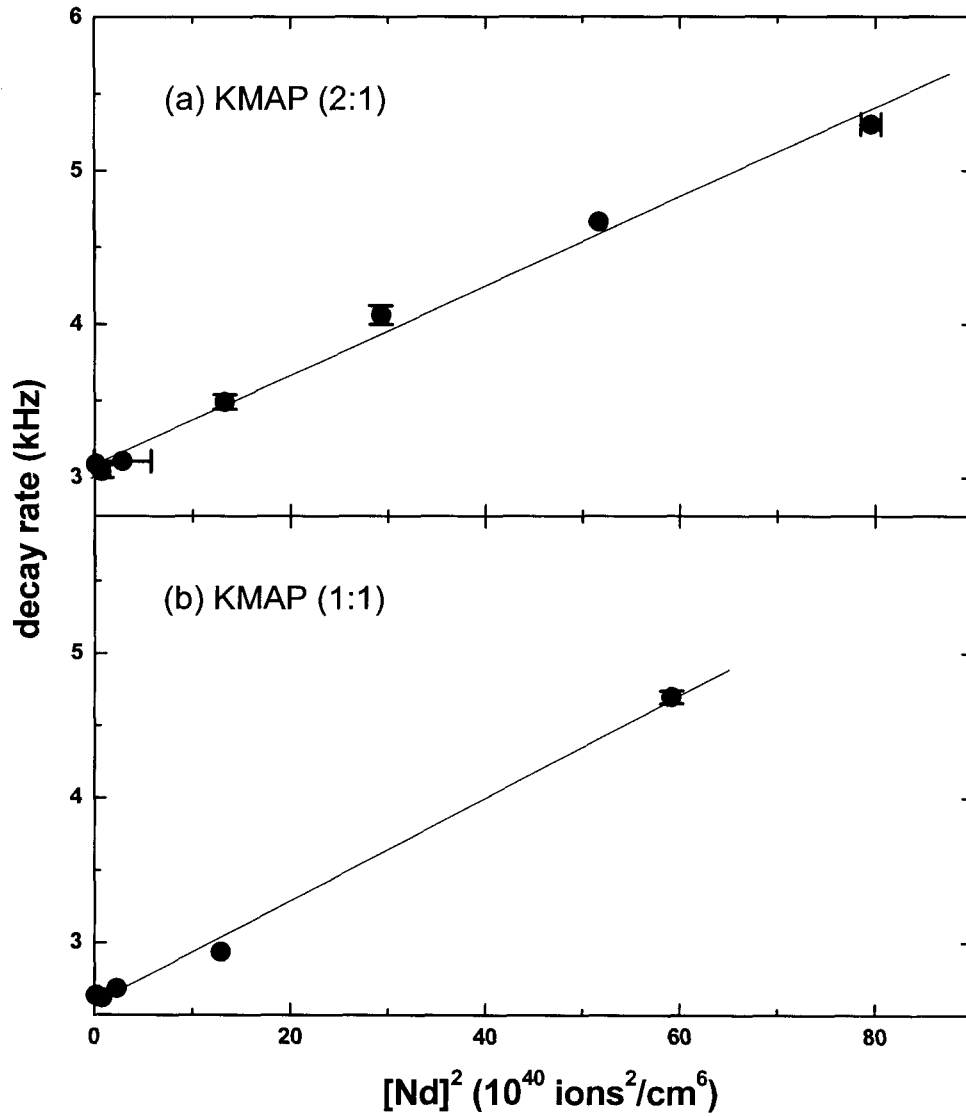


Figure 3. Measured non-radiative decay rate due to Nd self-quenching in KMAP (a) (2:1) and (b) (1:1) glasses. The lines are linear least-squares fits to the data; the measurement error is within the size of the symbols except where otherwise shown.

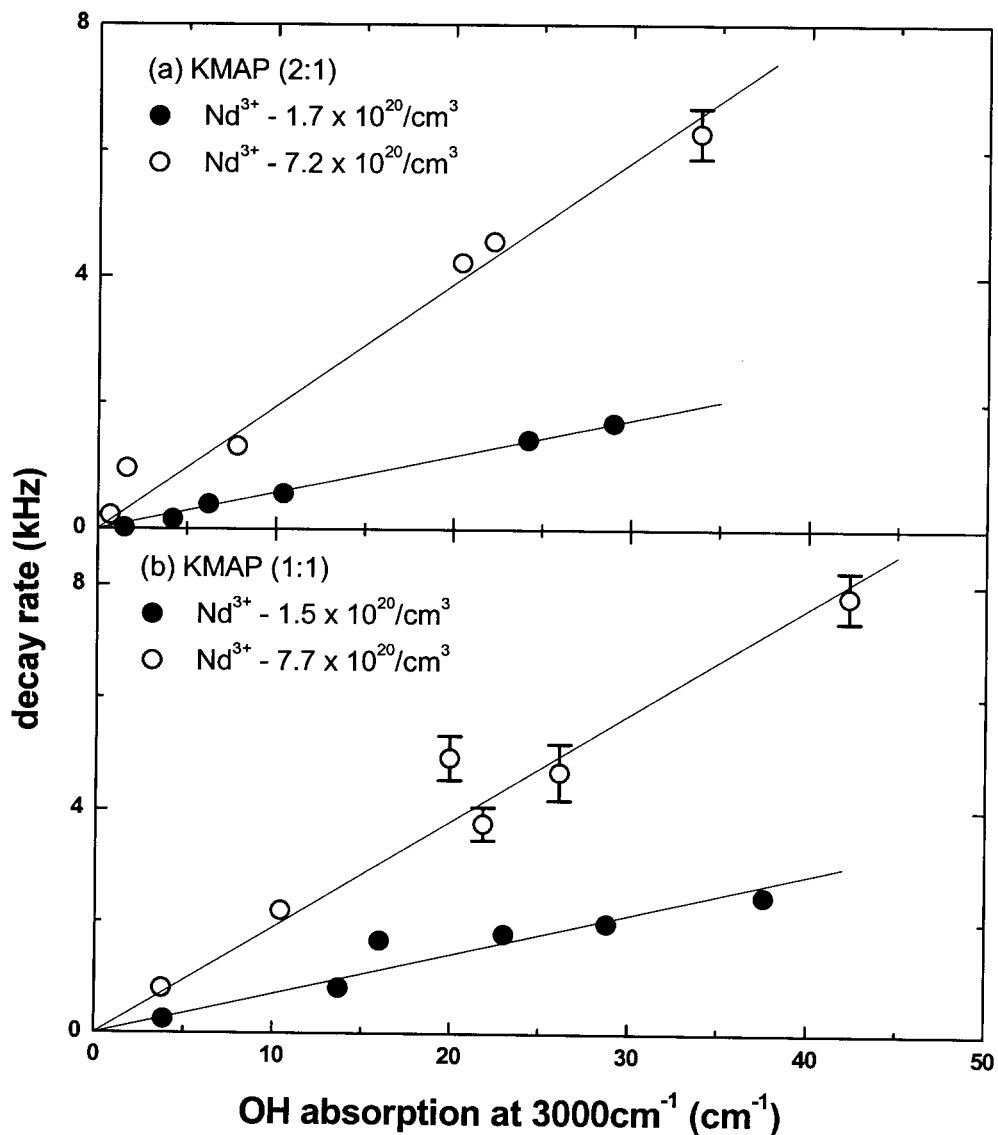


Figure 4. Non-radiative decay rate due Nd fluorescence quenching by OH in KMAP (a) (2:1) and (b) (1:1) glasses at two different Nd doping levels. The lines represent linear least squares fits to the data and the slopes are the fluorescence quenching rates ( $Q_{\text{OH}}$ ) per OH impurity concentration given as  $\text{Hz}/\text{cm}^{-1}$  absorption at  $3000\text{ cm}^{-1}$ .

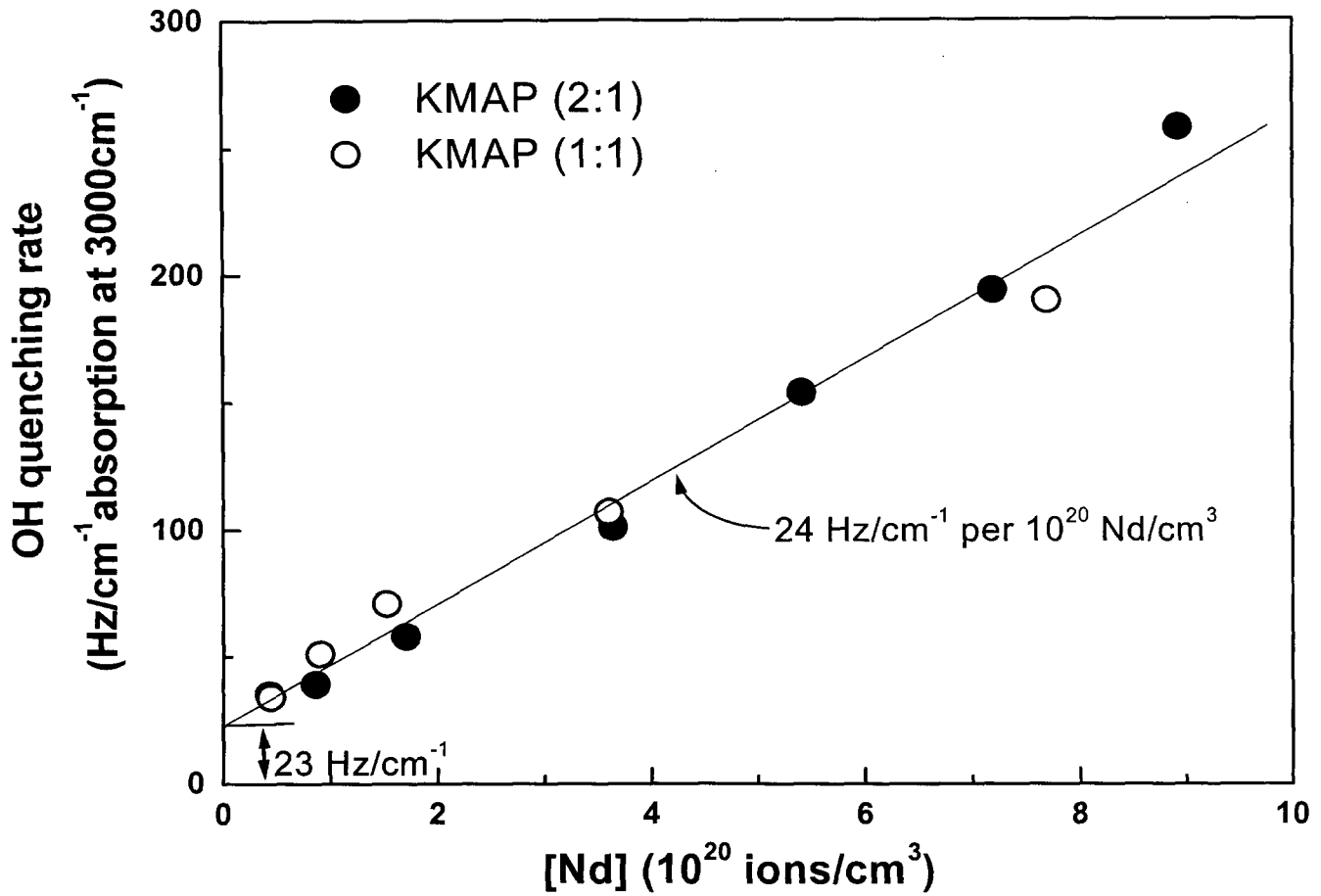


Figure 5. Nd fluorescence quenching by OH groups,  $Q_{OH}$ , as a function of Nd-doping concentration for both the KMAP (2:1) and (1:1) glasses. The line is a least squares fit to the data and has a slope of 24 Hz/cm<sup>-1</sup> per 10<sup>20</sup> Nd ions/cm<sup>3</sup> and a non-zero intercept of 23 Hz/cm<sup>-1</sup> where cm<sup>-1</sup> is the unit of the OH absorption coefficient at 3000 cm<sup>-1</sup>.

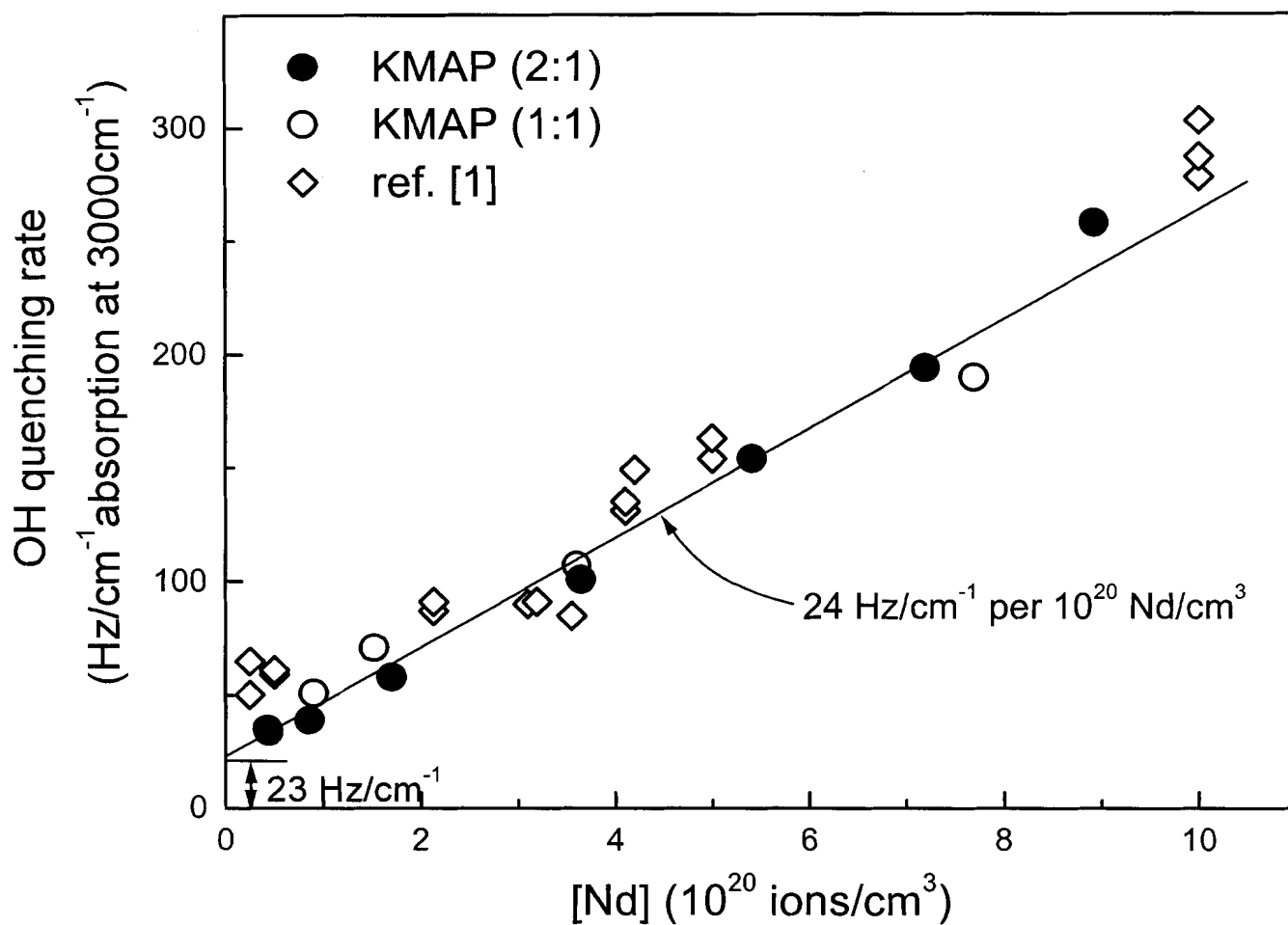


Figure 6. Comparison of the Nd quenching rates by OH reported here with data for eighteen other near-metaphosphate glasses as compiled elsewhere [1]; the solid line is from Fig 5.

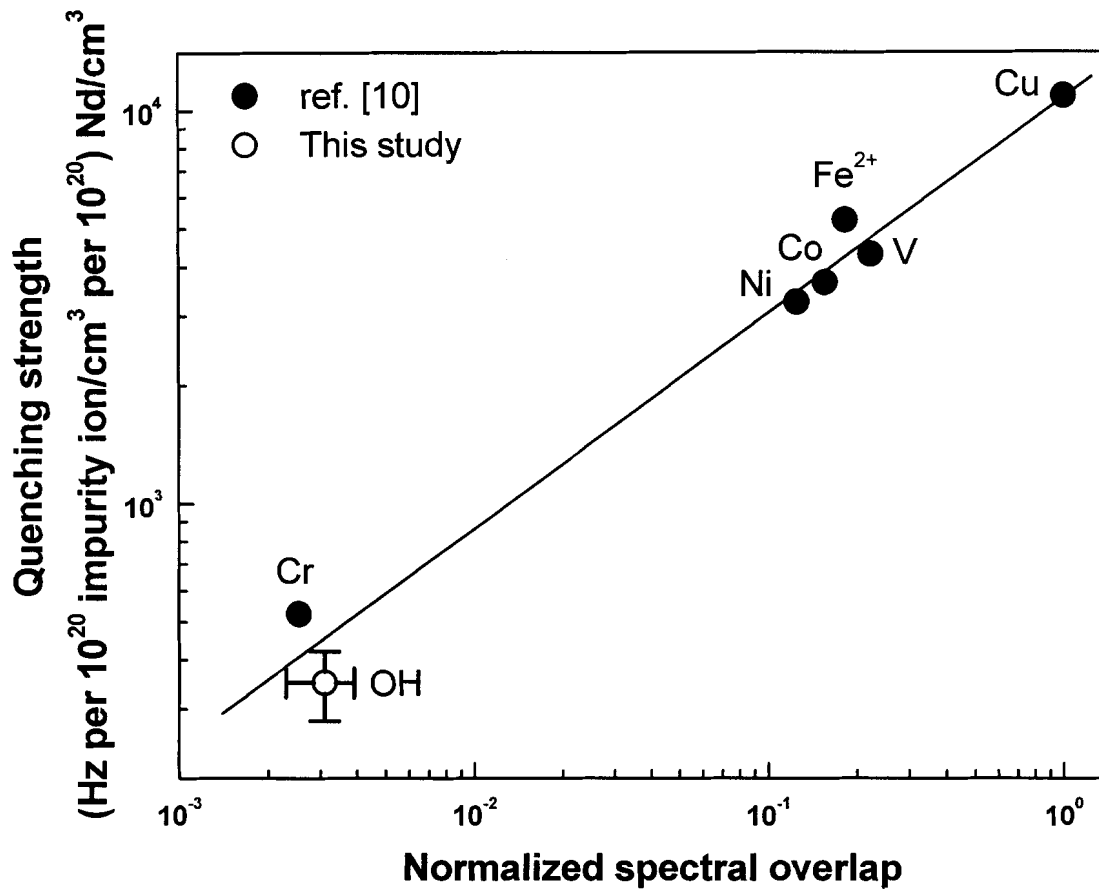


Figure 7. Strength of Nd-fluorescence quenching by OH and other common transition metal impurities in phosphate laser glass versus the spectral overlap with the  $^4F_{3/2}$  to  $^4I_J$  transitions (normalized to that for Cu); data for the metal ion impurities are from [10]. The units of the quenching strength are Hz per  $10^{20}$  impurity ions/cm<sup>3</sup> per  $10^{20}$  Nd ions/cm<sup>3</sup>.